Materials Science & Engineering A 565 (2013) 278–284

Contents lists available at SciVerse ScienceDirect

Materials Science & Engineering A

journal homepage: www.elsevier.com/locate/msea

# On the effect of hydrogen and Fe on reproducibility of tensile properties in cast Al–Si–Mg alloys

G. Eisaabadi B. [a,b,*], P. Davami [a], N. Varahram [a], S.K. Kim [b]

[a] Department of Materials Science and Engineering, Sharif University of Technology, Tehran, Iran
[b] Foundry Technology Center, Korea Institute of Industrial Technology, Incheon, South Korea

ARTICLE INFO

*Article history:*
Received 9 July 2012
Received in revised form
5 December 2012
Accepted 7 December 2012
Available online 14 December 2012

*Keywords:*
Al–Si–Mg alloys
Fe-rich phase
Porosity
Reproducibility
Weibull analysis

ABSTRACT

Gas porosities and Fe-rich phases and entrapped double oxide films (hereafter: oxides) are known to be the most detrimental defects in cast Al–Si–Mg alloys. The effects of H (gas porosities) and Fe (β-$Al_5FeSi$ phase) on reproducibility of tensile properties in Al–7Si–0.35Mg alloy have been investigated in this study. Four different casting conditions (Low H–Low Fe, Low H–High Fe, High H–Low Fe and High H–High Fe) were studied. In each case, 30 tensile test samples were prepared by casting in a metallic mold and machining (total of 120 tensile test samples). Results of tensile test were analyzed by Weibull three-parameter analyses. The microstructures of samples were studied by optical microscope. Total of 800 metallography images (200 images for each experiment) were taken and analyzed by image analysis software. Finally, the relationship between tensile properties and defects characteristics was discussed.

According to the results, Fe (β-$Al_5FeSi$ phase) showed considerably larger negative impact on tensile properties of the alloy compared to H (pores). Results of Weibull analysis revealed that the scattering of tensile properties was mainly due to the presence of β phase within the microstructure. Results of image analysis showed that the pore area% and number of pores/$cm^2$ were mainly controlled by H and Fe content of the melt, respectively. Also, it was shown that Weibull modules of UTS and El% increased linearly with increasing the shape factor of pores. Furthermore, tensile properties of the examined alloy showed strong dependence to the number of pores.



## 1. Introduction

Al–Si–Mg cast alloys offer a good combination of mechanical properties and castability, which explains their wide use in automotive and aerospace applications [1–4]. Nevertheless, aluminum castings have been rarely used in safety-critical applications due to concerns about the variability in mechanical properties, especially in elongation and fatigue life [1,2,5]. This high level of variability is the consequence of structural defects in castings, i.e. pores, Fe-rich phases and oxides, which degrade mechanical properties [6]; they cause premature fracture in tension [2,7] and fatigue [8], resulting in low ductility, tensile strength and fatigue life [9,10]. Therefore, the presence of major structural defects results in the high level of variability in mechanical properties [10,11], as evidenced most notably by lower Weibull module [2,12–14]. Hence, the minimization and even elimination of structural defects is vital for wider use of Al–Si–Mg castings in structural applications in aerospace and automotive industries.

Another important defect which occurs in cast aluminum alloys is gas porosities. Hydrogen is the only gas that is appreciably soluble in aluminum and its alloys. Actual liquid and solid solubilities in pure aluminum just above and below the solidus are 0.69 and 0.04 ppm [15]. These values vary only slightly for most cast aluminum alloys. During cooling and solidification, precipitation of the hydrogen results in formation of primary and/or secondary voids. Many researchers [16–20] investigated the effect of porosities on mechanical properties of cast Al–Si–Mg alloys. It has been suggested that porosity is a leading cause in the reduction of mechanical properties, particularly elongation and fatigue resistance, as well as a loss of pressure tightness and a degradation of the surface appearance in cast parts [15]. Liu et al. [21] claimed that oxides have deleterious effect over the mechanical properties whereas Wang et al. [22] suggested that porosity is more detrimental than oxides.

Iron is the most common impurity that can be found in cast aluminum alloys since it cannot be removed economically [23]. In the Al–Si–Fe system there are five main Fe-rich phases: $Al_3Fe$, α-$Al_8Fe_2Si$, β-$Al_5FeSi$, δ-$Al_4FeSi_2$ and γ-$Al_3FeSi$ [24]. In addition, Fe and Mg may result in the appearance of π-$Al_8Mg_3FeSi_6$. Therefore, α, β and π phases are normally precipitated in cast hypoeutectic and eutectic aluminum alloys containing magnesium [25]. Many researchers reported that increasing of iron content decreases the mechanical properties of cast Al–Si alloys [26–30].

* Correspondence to: Eco metal Laboratory, Foundry Technology Center, Korea Institute of Industrial Technology, 7-47, Songdo-Dong, Yeonsu-Gu, Incheon 406-840, South Korea. Tel.: +82 32 8500 417.
*E-mail addresses:* G_eisaabadi@mehr.sharif.ir, G_eisaabadi@kitech.re.kr, rasol121@gmail.com (G. Eisaabadi B.).

0921-5093/$ - see front matter © 2012 Elsevier B.V. All rights reserved.
http://dx.doi.org/10.1016/j.msea.2012.12.022

Several researchers investigated the different interactions between pores and Fe-rich phases in cast aluminum alloys [31–34]. It has been suggested [31] that, increasing the iron content in the cast Al–A319 alloy increased the porosity, particularly shrinkage porosity. It is due to the precipitation of long and thick (needle or platelet) β-$Al_5FeSi$ phases which are often branched into several needles. The branched morphology of β phase decreases the permeability of the interdendritic network [31,34,35] and results in reduced feeding of liquid metal through the interdendritic channels. Subsequently, the tendency for formation of extended porosity defects within the castings will be increased [35]. The nucleation of porosity on β phase is more important in sand mold castings, where the slower cooling rates favor the formation of β phase [32]. Taylor et al. [34] suggested two mechanisms for the role of iron in porosity formation. The first theory suggests that the β platelets form in the interdendritic channels during solidification and cause a physical restriction to the movement of compensatory feed liquid. This results in inadequate feeding and favors the formation of porosity. The second theory considers the β phases as active pore nucleation sites that physically constrain the growth of the pores and influenced their ultimate shape.

From the above literature survey, pores and Fe-rich phases are two of the main defects that influence the tensile properties of cast Al–Si–Mg alloys. On the other hand, these defects represent a complicated interaction with each other. Therefore, the aim of this study is to investigate the effect of these defects on tensile properties of Al–Si–Mg alloys and their effects on reproducibility of tensile properties in these alloys.

## 2. Experimental procedure

The alloy used in this experiment was a 2L99 alloy with a specific chemical composition of 7.2 wt% Si, 0.35 wt% Mg and 0.09 wt% Fe that was received as 5 kg ingots. The alloy was divided into two groups, with low and high Fe contents. The Fe content of low and high Fe alloys was designed to be 0.1 and 0.8 wt%, respectively. Al-20 wt% Fe master-alloy was added into the 2L99 molten alloy in order to increase the Fe content of the alloy. Table 1 shows the actual chemical composition of the investigated alloys (sample was taken from the melt), which was analyzed by ICP–AES (inductively coupled plasma–atomic emission spectroscopy).

The pattern used in this study, was tensile test bar mold shown in Fig. 1. The dimensions of the gating system are listed in Table 2. This mold was designed based on the naturally pressurized running system. According to Table 2, the runner height after filter that is indicated in Fig. 1 was 12 mm. This height was determined with considering the melt critical velocity. According to this theory, the critical velocity has been shown both theoretically and experimentally to be approximately 0.50 m/s for liquid aluminum alloys [36,37]. This states that, if the molten aluminum flows with velocity greater than 0.50 m/s, then there will be surface turbulence and the probability of oxide generation, which will then be incorporated into the bulk of the liquid metal [38].

On the other hand, it was shown that if a stream of melt falls from the height of $\boldsymbol{h}$, the melt velocity, $\boldsymbol{v}$, could be calculated by Eq. (1) [36]:

$$v = (2gh)^{1/2} \tag{1}$$

where; the gravitational acceleration ($\boldsymbol{g}$) is 9.81 m/s$^2$, then the distance $\boldsymbol{h}$, in millimeters, that the metal has to fall to reach the critical velocity is given by Eq. (2):

$$\boldsymbol{h} = \boldsymbol{v}^2/2\boldsymbol{g} = 0.52/(2 \times 9.8) = 12.7 \text{ mm} \tag{2}$$

since, the runner height of the mold was 12 mm (less than 12.7 mm), the velocity of free falling melt was 0.48 m/s (less than critical value). Therefore, these castings had no or very small amount of entrapped oxides. Furthermore, in all castings, a 30 ppi ceramic filter was placed in the filter print. Ardekhani and Raiszadeh [2] showed that a 30 ppi ceramic foam filter can remove almost all previously formed inclusions and oxides, and also reduce the speed of flow of the molten alloy filling the mold in order to prevent further oxide from being entrained.

In order to control the hydrogen content of the melt, in castings with Low H, a rotary fluxing and degassing machine was used to obtain a Low H content (rotor speed 150 rpm, flux

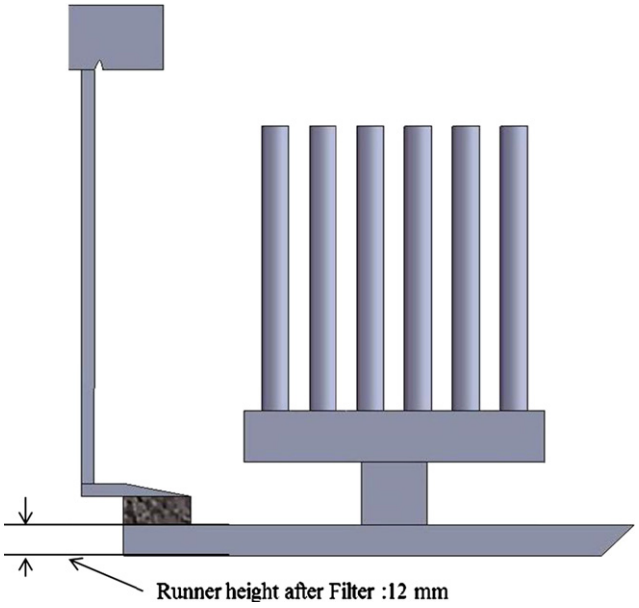


**Fig. 1.** Geometry of pattern used in this study (after [39]).

**Table 2**
Dimensions of running system component in Fig. 1 (all in millimeter) [39].

| Running system component | Dimensions |
|---|---|
| Pouring basin | 50 × 70 (depth 60) |
| Sprue cross section | Up (10 × 45), down (9 × 13) |
| Sprue height | 320 |
| Filter print | 50 × 50 × 22 |
| Runner cross section | Before filter (11 × 14), after filter (12 × 14) |
| Gate cross section | 11 × 48.4 |
| Riser | 220 × 40 × 40 |
| Tensile samples | Height 220, diameter 20 |

**Table 1**
The chemical composition of investigated alloys.

| | Si | Mg | Fe | Ti | Cu | Ni | Zn | Sn | Mn | Al |
|---|---|---|---|---|---|---|---|---|---|---|
| Low Fe | 6.98 | 0.35 | 0.09 | 0.15 | 0.01 | 0.013 | < 0.015 | < 0.005 | < 0.005 | Balance |
| High Fe | 7.01 | 0.34 | 0.85 | 0.14 | 0.01 | 0.016 | < 0.015 | < 0.005 | < 0.005 | Balance |

**Table 3**
Different casting conditions investigated in the present study.

| H | Fe | Designation | H content (ml/100 g of melt) | Fe content |
|---|---|---|---|---|
| Low | Low | LL | 0.11 | 0.09 |
| | High | LH | 0.10 | 0.85 |
| High | Low | HL | 0.43 | 0.09 |
| | High | HH | 0.45 | 0.85 |

feed rate 18 g/min. and injection time 200 second). The H measurement was performed using a HyScan II (a product from Severn System Company). On the other hand, for castings with High H, no degassing was carried out. Therefore, four different melt was prepared according to Table 3; with two levels of hydrogen and Fe.

The pouring temperature was 750 °C for all experiments. In all cases, the melt was carefully skimmed to remove oxides and inclusions from surface of the melt. The alloy was carefully poured into a mold, which had already been placed in a roll-over device. Immediately after pouring, the mold was slowly rotated through 180° and left for about 10 min, to ensure directional solidification of the test bars towards the runner bars, which would now be acting as feeders, and hence solidification shrinkage in the test bars was avoided. Five molds were poured in each case, giving 30 test bars, for each experiment in Table 3.

After casting, the test bars were heat treated according to T6 condition using the following schedule [4]:

- Solution treated at 540 °C for 10 h in an air circulating furnace;
- Water quenched at 60 °C;
- Naturally aged at room temperature for 24 h;
- Artificially aged at 165 °C for 12 h.

After heat treatment, the samples were machined according to British Standard (BS EN 10002-1: 2002) [BSI 2001], to dimensions of 6.75 mm diameter and 25 mm gauge length on a 40 mm parallel length. Tensile testing was done with an Instron 1195-5500R machine with a cross-head speed of 1 mm/min. The elongation of the sample was determined from the load–displacement curves derived from the cross head movement of the machine.

A Weibull analysis was carried out to determine the reproducibility of the properties obtained from each casting condition. The Weibull analysis is a convenient way to determine the dispersion of mechanical properties [4,14,39–42]. It is more accurate than standard deviation, which assumes symmetrical distribution of data about a mean value [43,44]. Green and Campbell [12] concluded that the Weibull distribution most accurately describes the distribution of tensile properties. For aluminum castings, the two and three-parameter forms of Weibull distribution is widely adopted [13,45]. The cumulative probability function of the three-parameter Weibull distribution is expressed as Eq. (3) [46]:

$$P = 1-\exp\left(-(\sigma-\sigma_T)/\sigma_C\right)^m \quad (3)$$

where $P$ is the probability of failure at a given stress (strain, fatigue life, etc.) $\sigma$ or lower. The threshold value $\sigma_T$ is the value below which no specimen is expected to fail. The term $\sigma_C$ is the characteristic stress at which $1/e$ of specimens survived. It is similar to a mean value in representation of a set of normally distributed data [13,39]. "$m$" is the shape parameter, which is alternatively referred as the Weibull modulus. Taking the logarithm of Eq. (3) twice gives

$$\ln[-\ln(1-P)] = m\ln(\sigma-\sigma_T) - m\ln(\sigma_C) \quad (4)$$

The Weibull module "$m$" is therefore the slope of a plot of $\ln[-\ln(1-P)]$ against $\ln(\sigma-\sigma_T)$, where $P$ is a measure of the probability of failure for the $n^{th}$ sample [45]. $P$ can be estimated in various ways. It has been proposed [43] that the following estimator gave the most accurate determination of the probability of failure ($P$):

$$P = (n-0.5)/N \quad (5)$$

where $n$ is the rank in an ascending fashion and $N$ is the total number of samples. The Weibull module "$m$" is therefore a single value that shows the spread of properties. Higher Weibull module indicates a narrower scattering of properties. In case of castings, the higher Weibull module indicates castings with lower number of defects and a greater reproducibility of properties [2,4,12–14,39].

The goodness of fit of Weibull line and experimental data was evaluated using Eq. (6) [47] which gives the critical values for $R^2_{0.05}$. This critical value can be used to evaluate the goodness-of-fit. If $R^2$ of the linear regression from the Weibull probability analysis is less than $R^2_{0.05}$, it can be concluded that the data does not come from a Weibull distribution. On the other hand, If $R^2 \geq R^2_{0.05}$, the scattering of properties is according to the Weibull distribution (Weibullian). In the present study, since the value of $n$ (number of samples) was 30, therefore, the value of $R^2_{0.05} = 0.91324$.

$$R^2_{0.05} = 1.0637 - 0.4174/n^{0.3} \quad (6)$$

To investigate the effects of initial H content and Fe on morphology of defects (pores), the microstructure of test bars was investigated by optical microscope. Using standard metallography procedure, 10 metallography specimens were prepared for each experimental condition. Subsequently, 20 random pictures were taken from microstructure of each specimen (total of 200 metallography pictures for each condition at magnification of 50X). The images that obtained for each experiment were analyzed by Digimizer image analysis software (a product from MedCalc Software). From the results of image analysis, the fraction of pores area% (**FP**%), number of pores/cm$^2$ (**pore density**) and average shape factor of pores (**SF**) were determined. As might be expected, many different Fe-rich phases were present within the microstructure of samples. However, since the β phase was the dominant Fe-rich phase, the surface fraction of this phase was measured by image analysis of the microstructure of the samples obtained in each experiment. To do this, 250 images from microstructure of samples in each experiment were analyzed by image analysis software.

## 3. Results and discussions

### 3.1. Tensile properties

Fig. 2(a and b) represents the tensile properties that obtained from each experimental condition. In term of UTS data (Fig. 2a), the maximum and minimum values correspond to experiments with lowest (LL) and highest (HH) defect content, respectively. Also, it is depicted that regardless of H content, the High Fe experiments (LH and HH) showed the lower values of UTS than High Fe experiments (HL and HH). In term of El% data (Fig. 2b), increasing of either H or Fe resulted in considerable decrease of El%. Also, it can be seen that the Low Fe experiments (LL and HL) showed considerably lower standard deviation% than High Fe experiments (LH and HH). Although it seems that the Low H–Low Fe (LL) experiment had a very wider range of variation in El% data,

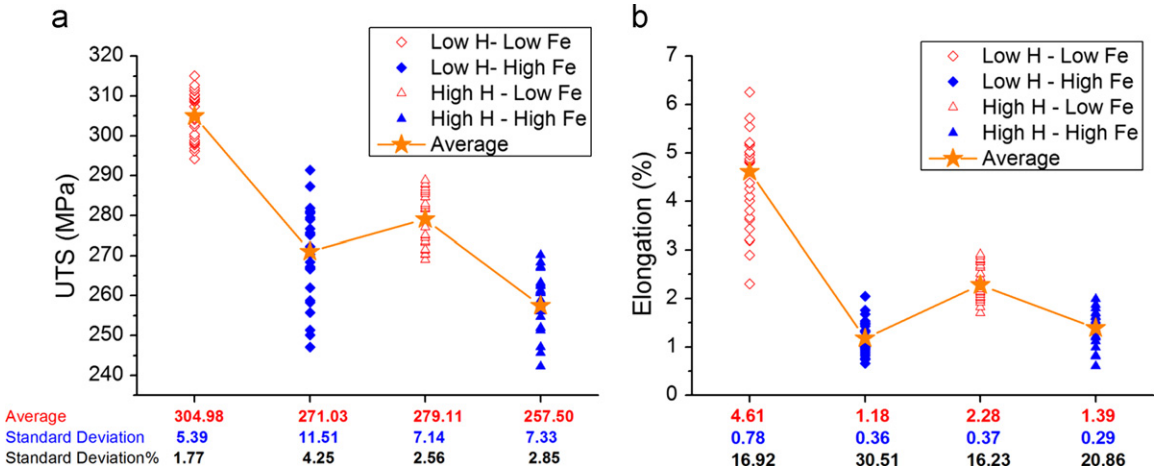


**Fig. 2.** (a) UTS and (b) El% data obtained from different experiments. Standard deviation %=(standard deviation/average) × 100.

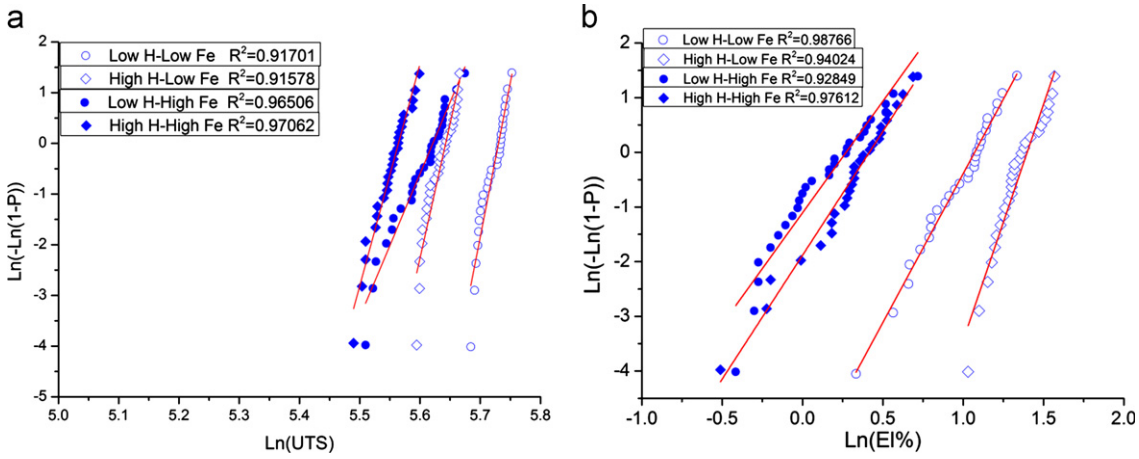


**Fig. 3.** Weibull plots of (a) UTS and (b) El% data obtained from different experimental conditions.

this experiment corresponds to the lowest standard deviation % among all samples. This example clearly indicates that using of single analysis (i.e. standard deviation, standard deviation% or even the graphs that show the distribution of a measured property or quantity) could not reveal the effects of different parameters completely. Therefore, it is necessary to utilize other techniques for interpretation of the results. In this study, we used Weibull analysis to evaluate the scattering of the tensile properties of the alloy. From Fig. 2(a and b), increasing of only H content (from LL to HL) decreased the UTS and El% by about 8.48 and 50.54%, respectively. On the other hand, increasing of only Fe content (from LL to LH) decreased the UTS and EL% by about 11.13 and 74.40%, respectively. Therefore, it can be seen that Fe was the main parameter that depressed the tensile properties, especially the El%.

### 3.2. Weibull analysis

Fig. 3(a and b) shows the Weibull plots of UTS and EL% data obtained for each experiment, respectively. Also the corresponding linear fit and adjust *R*-square values of fitted lines are shown in these figures. From Fig. 3(a and b)

- The Adjust *R*-squares of all fitted lines (both UTS and El% data) was higher than critical adjust *R*-square ($R^2_{0.05}=0.91324$) that obtained from Eq. (6). This indicates that the data were distributed in a Weibullian manner and no further analysis (i.e. Weibull mixture analysis) was required.
- The Weibull plots of High Fe experiments (LH and HH) shifted to lower values of UTS and El% compared to Low Fe experiments (LL and HL).

**Table 4**
Summary of the Weibull analysis.

| Data set | Parameter | Low H Low Fe | Low H High Fe | High H Low Fe | High H High Fe |
|---|---|---|---|---|---|
| UTS | Threshold | 5.7 | 5.6 | 5.6 | 5.5 |
| | Characteristic | 308.0 | 276.2 | 282.2 | 261.0 |
| | Module | 62.5 | 28.5 | 51.9 | 41.8 |
| El% | Threshold | 1.57 | 0.27 | 0.90 | 0.40 |
| | Characteristic | 4.80 | 1.31 | 2.46 | 1.50 |
| | Module | 7.8 | 3.6 | 5.6 | 5.0 |

Results of Weibull analysis are summarized in Table 4 and Fig. 4 represents the variation of the Weibull modules of UTS and El% graphically. From Table 4 and Fig. 4(a), increasing Fe (form LL to LH) and H contents (from LL to HL) decreased the Weibull module of UTS by 54.4 and 16.96%, respectively. Also from Table 4 and Fig. 4(b), increasing of Fe (form LL to LH) and H contents (from LL to HL) decreased the Weibull module of El% by 53.84 and 28.2%, respectively. Therefore, Fe had considerably larger negative

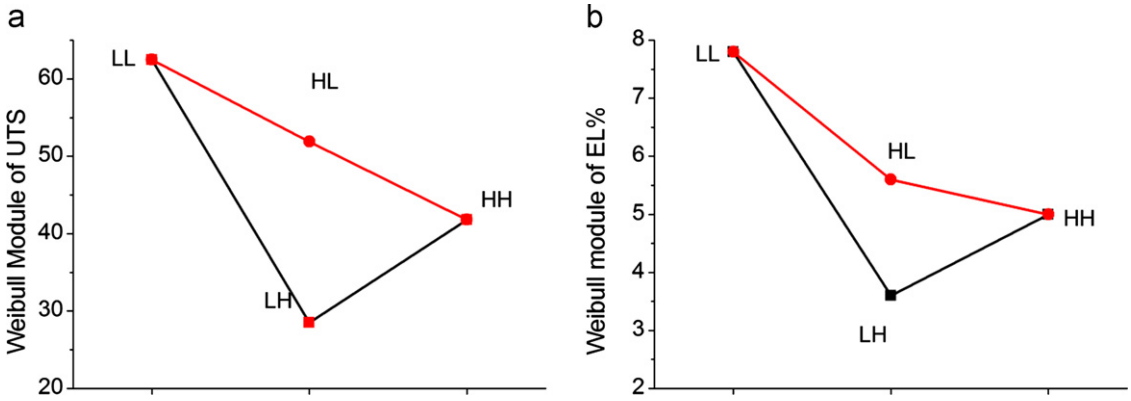


**Fig. 4.** Graphical representation of the results of Weibull analysis of (a) UTS and (b) El% data.

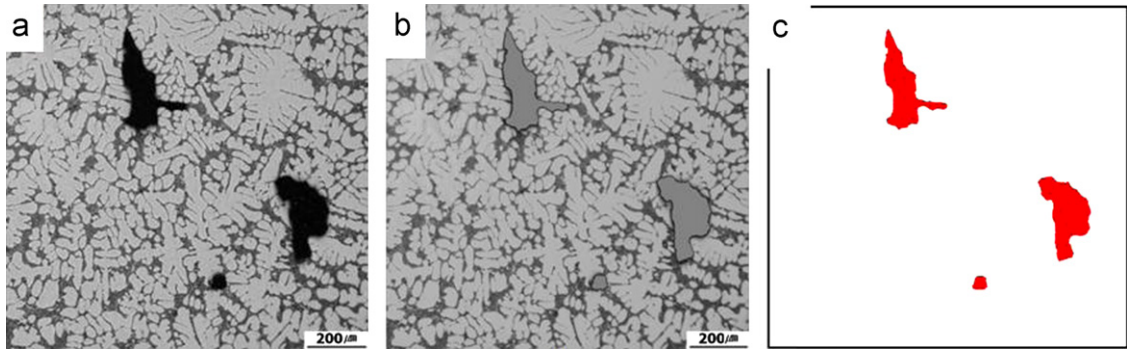


**Fig. 5.** Typical microstructure that was analyzed using image analysis software. (a) Original microstructure, (b) Original microstructure overlaid with binary image of pores and (c) the final binary image of (a).

impact on scattering of tensile properties than H. Also, it can be seen that increasing of Fe content resulted in further decrease of UTS and El% Weibull modules from (HL to HH). In Fig. 4(a and b), it is interesting to notice that increasing of H to the samples that already had high amount of Fe (LH experiment), increased the Weibull modules of UTS and El% (from LH to HH). Unfortunately, this increase of Weibull modules of UTS and El% has no practical benefits, since the increasing of H in High Fe samples results in decrement of UTS from 271 to 257 MPa (Fig. 2). The increase in Weibull module of UTS and El% from LH to HH samples is discussed in Section 3.3.

### 3.3. Study of microstructure and image analysis

Fig. 5(a) shows a typical image that obtained from a HL sample and Fig. 5(b and c) shows the Fig. 5(a) after processing (binarization) by image analysis software. The gray areas in Fig. 5(b) (red areas in Fig. 5c) are identified as pores by software. Table 5 shows the summary of the results obtained from image analysis for each experiment.

From the results of image analysis in Table 5, the FP% of Low H experiments (LL an LH) is considerably lower than High H experiments (HL and HH). Therefore, it is clear that the variations of FP% were mainly due to the variation in H content of the melt. In this table, the High Fe experiments (LH and HH) showed higher density of pores than Low Fe experiments (LL and LH). Therefore the main factor that influenced the density of pores was Fe content. Also, it can be seen that SF decreased with increasing the Fe content (from LL to LH and HL to HH).

It is interesting to notice that the SF increased with increasing the H content of the melt in High Fe samples (from LH to HH). This explains that why the Weibull modules of both UTS and El% of HH sample were higher than LH samples. In the author's

**Table 5**
Results of image analysis.

| H | Fe | Exp. | FP% | Number density of pores ($cm^{-2}$) | SF | Surface fraction of the β phase (%) |
|---|---|---|---|---|---|---|
| Low | Low | LL | 0.36 | 1007 | 0.45 | 0.11 |
| | High | LH | 0.41 | 1603 | 0.36 | 3.62 |
| High | Low | HL | 2.41 | 1301 | 0.42 | 0.16 |
| | High | HH | 4.79 | 3620 | 0.40 | 3.51 |

previous work [14], it has been suggested that the diffusion of H into the pores expands them and changes their morphology from planar to spherical (increase the SF). They simulated the effects of this morphological change on maximum Von Misses stress and equivalent plastic strain around the pores and showed that both maximum Von Misses stress and equivalent plastic strain decreased with increasing the SF of pores. This decreased maximum Von Misses stress and maximum equivalent plastic strain decreased the scattering of tensile properties and resulted in higher Weibull module of UTS and El% in samples with high amount of dissolved H (as shown in Section 3.2).

### 3.4. Relationship between defects, tensile properties and reliability

In this section, the relationships between characteristics of the pores (FP%, density and SF of pores from Table 5) and tensile properties (namely UTS and El % from Table 4) and reliability (Weibull module of UTS and El % from Table 5) are discussed.

Fig. 6(a–c) represents the variations of UTS, El% with FP%, density and SF of pores, respectively. It can be seen that there was no clear relationship between the FP% and tensile properties (Fig. 6a). Fig. 6(b) shows that the tensile properties of the alloy

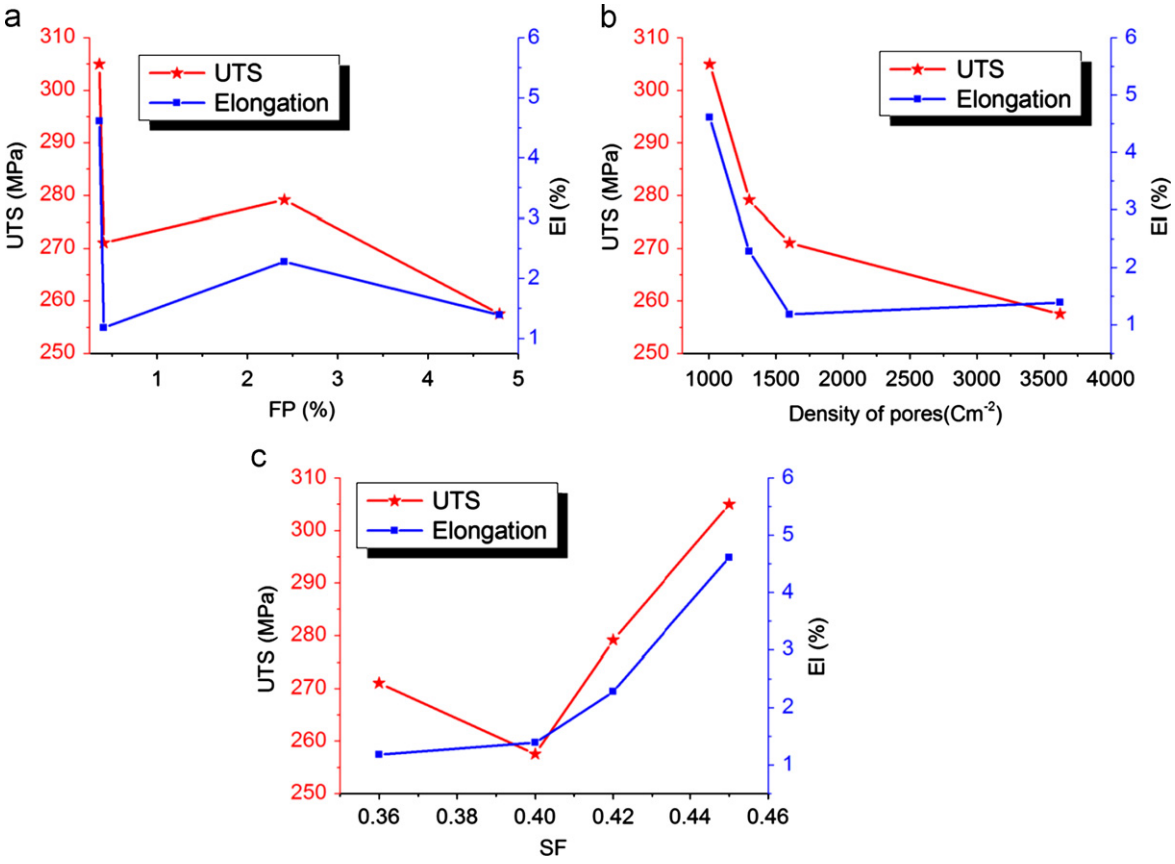


**Fig. 6.** Variations of tensile properties with (a) FP%, (b) density and (c) SF of pores.

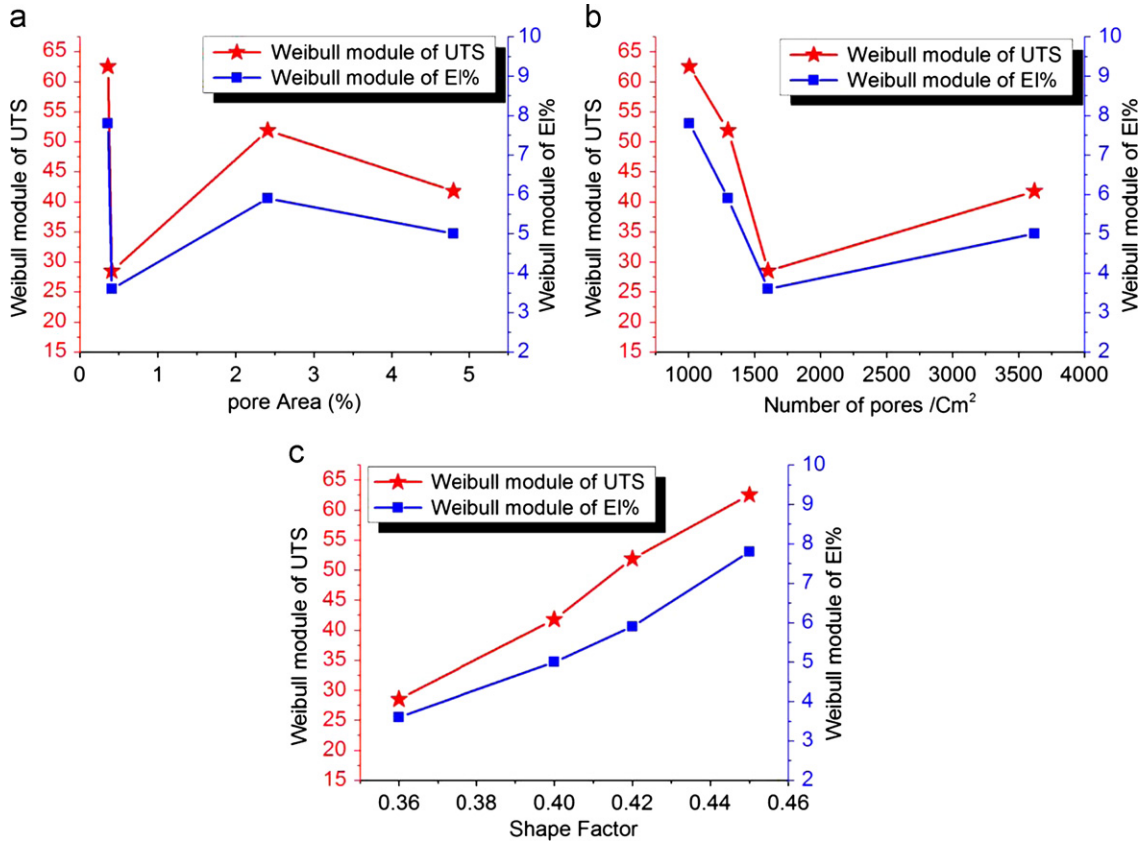


**Fig. 7.** Variations of Weibull modules of UTS and EI% with (a) FP%, (b) density and (c) SF of pores.

decreased with increasing the density of pores. From this figure, increasing the density of pores to values less than 1600 resulted in sharp decrease of tensile properties. On the other hand, in pore densities larger than 1600, the tensile properties of the alloy changed slightly with increasing pore density. Fig. 6(c) shows that there was no clear relationship between the UTS and SF, but the El% of samples increased with increasing the SF.

Fig. 7(a–c) represents the variations of Weibull modules of UTS and El% with FP%, density and SF of pores, respectively. Fig. 7(a and b) shows that there was no relationship between Weibull modules of UTS and El% with FP% and density of pores, respectively. On the other hand, Fig. 7(c) shows that Weibull modules of UTS and El%, increased almost linearly, with increasing of the shape factor of pores.

## 4. Conclusions

From the present study the following conclusions can be drawn:

- Increasing of both H and Fe contents of the melts decreased the tensile properties of examined alloys.
- The Fe-related defects (Fe-rich phase) showed the larger negative effect on UTS and El% of examined alloys than hydrogen.
- A clear relationship was found between the number density of pores and the tensile properties of the alloy (UTS and El%). It was shown that the tensile properties of the alloy decreased with increasing the number density of pores. The reduction of the tensile properties of the alloy with number density of pores is directly related to the formation of β Fe-rich. The β platelets restrict the flow of liquid metal through the inter-dendritic feeding paths and favor the formation of shrinkage porosity. The shrinkage porosities with irregular shape act as effective stress riser sites and therefore, impair the tensile properties of the alloy.
- The Weibull modules of UTS and El% of High Fe samples increased with increasing the level of dissolved H (from LH samples to HH samples). The authors suggest that this is due to the diffusion of the hydrogen into the pores in High H samples that changes their morphology from two dimensional to three dimensional. This morphological evolution decreases the shape irregularity of pores, which in turn, decreases the severity of stress concentration around the pores and increases the Weibull modules of UTS and El% of the alloy.
- The Weibull modules of UTS and El% decreased with increasing the both Fe and H contents of the melt, but Fe showed considerably larger negative impact than H.
- The Weibull modules of UTS and El% increased linearly with increasing the SF of pores. The Higher SF means less irregular pores with less stress concentration factor around them that in turn, increases the Weibull modules of UTS and El%.
- It was shown that the El% of samples increased with increasing the shape factor of pores.

## Acknowledgment

One of the authors (G. Eisaabadi B.) wishes to acknowledge the financial support of the Ministry of Science, Research and Technology of the Islamic Republic of Iran and Korean Institute of Industrial Technology's (KITECH, Incheon, South Korea) for their financial supports and staffs at Razi metallurgical Research Center (Tehran, Iran) and Casting and Solidification Lab. of Sharif University of Technology for their help during the experiments. He also wants to appreciate Professor John Campbell (University of Birmingham) for his constructive discussions during the interpretation of the results.

## References

[1] M. Tiryakioğlu, J. Campbell, N.D. Alexopoulos, Metall. Mater. Trans. A 40 (2009) 1000–1007.
[2] A. Ardekhani, R. Raiszadeh, J. Mater. Eng. Perform. (2011) 1–11.
[3] M. Aryafar, R. Raiszadeh, A. Shalbafzadeh, J. Mater. Sci. 45 (2010) 3041–3051.
[4] G. Eisaabadi B., N. Varahram, P. Davami, S.K. Kim, Mater. Sci. Eng. A 548 (2012) 99–105.
[5] J. Mi, R. Harding, J. Campbell, Metall. Mater. Trans. A 35 (2004) 2893–2902.
[6] J. Campbell, Metall. Mater. Trans. A 37 (2006) 857–863.
[7] M. Tiryakiolu, J. Campbell, J. Staley, Scr. Mater. 49 (2003) 873–878.
[8] C. Nayhumwa, N. Green, J. Campbell, Metall. Mater. Trans. A 32 (2001) 349–358.
[9] J.T. Staley, M. Tiryakioğlu, J. Campbell, Mater. Sci. Eng. A 465 (2007) 136–145.
[10] Y.J. Chen, H.Y. Teng, Y.T. Tsai, J. Mater. Eng. Perform. 13 (2004) 69–77.
[11] R. Raiszadeh, W. Griffiths, Metall. Mater. Trans. B 37 (2006) 865–871.
[12] N. Green, J. Campbell, Mater. Sci. Eng. A 173 (1993) 261–266.
[13] X. Dai, X. Yang, J. Campbell, J. Wood, Mater. Sci. Eng. A 354 (2003) 315–325.
[14] G. Eisaabadi B., P. Davami, S.K. Kim, N. Varahram, Mater. Sci. Eng. A 558 (2012) 134–143.
[15] J. Anson, J. Gruzleski, Mater. Charact. 43 (1999) 319–335.
[16] Z. Ma, A. Samuel, F. Samuel, H. Doty, S. Valtierra, Mater. Sci. Eng. A 490 (2008) 36–51.
[17] C. Tekmen, I. Ozdemir, U. Cocen, K. Onel, Mater. Sci. Eng. A 360 (2003) 365–371.
[18] M. Irfan, D. Schwam, A. Karve, R. Ryder, Mater. Sci. Eng. A 535 (2011) 108–114.
[19] Z. Lei, L. Hengcheng, P. Ye, W. Qigui, S. Guoxiong, Res. Dev. 8 (2011) 14–18.
[20] D. Dispinar, S. Akhtar, A. Nordmark, F. Syvertsen, M. Di Sabatino, L. Arnberg, Adv. Mater. Res. 445 (2012) 283–288.
[21] L. Liu, A. Samuel, F. Samuel, H. Doty, S. Valtierra, J. Mater. Sci. 38 (2003) 1255–1267.
[22] Q. Wang, P. Crepeau, C. Davidson, J. Griffiths, Metall. Mater. Trans. B 37 (2006) 887–895.
[23] Z. Li, A. Samuel, F. Samuel, C. Ravindran, S. Valtierra, H. Doty, Mater. Sci. Eng. A 367 (2004) 96–110.
[24] P. Skjerpe, Metall. Mater. Trans. A 18 (1987) 189–200.
[25] X. Cao, Heat Treatment of Liquid Metal, Precipitation and Sedimentation Processing of Liquid Al–11.5Si–0.4Mg Alloy, University of Birmingham, Birmingham, 2001.
[26] M. Ravi, U.T.S. Pillai, B. Pai, A. Damodaran, E. Dwarakadasa, Metall. Mater. Trans. A 33 (2002) 391–400.
[27] S. Shabestari, T. Mahmudi, M. Emamy, T. Campbell, Int. J. Cast Met. Res. 15 (2002) 17–24.
[28] R. Sinfield, D. Harris, J. Aust. Inst. Met. 20 (1975) 44–48.
[29] A. Mohamed, A. Samuel, F. Samuel, H. Doty, Mater. Des. 30 (2009) 3943–3957.
[30] S. Seifeddine, I.L. Svensson, Mater. Des. 31 (2010) 6–12.
[31] C. Villeneuve, A. Samuel, F. Samuel, H. Valtierra, S. Doty, in, 2001, pp. 1–14.
[32] N. Roy, A. Samuel, F. Samuel, Metall. Mater. Trans. A 27 (1996) 415–429.
[33] M.O. Otte, S.D. McDonald, J.A. Taylor, D.H. StJohn, W. Schneider, AFS Trans. 107 (1999) 471–478.
[34] J. Taylor, G. Schaffer, D. StJohn, Metall. Mater. Trans. A 30 (1999) 1643–1650.
[35] M.O. Otte, S.D. McDonald, J.A. Taylor, D.H. StJohn, W. Schneider, Trans. AFS 107 (1999) 471–478.
[36] M. Jolly, JOM 57 (2005) 19–28.
[37] J. Campbell, Castings, Butterworth-Heinemann, Oxford, UK, 2003.
[38] C. Caceres, L. Wang, D. Apelian, M. Makhlouf, Trans. AFS 107 (1999) 239–247.
[39] H. Hashemi, R. Raiszadeh, J. Appl. Sci. 9 (2009) 2115–2122.
[40] C.W.M. Nayhumwa, Influence of oxide film filling defects on fatigue properties of cast Al–7Si–Mg alloy, University of Birmingham, Birmingham, 1997.
[41] C. Nyahumwa, Afr. J. Sci. Technol. 6 (2010) 43–54.
[42] M. Cox, R. Harding, J. Campbell, Mater. Sci. Technol. 19 (2003) 613–625.
[43] A. Khalili, K. Kromp, J. Mater. Sci. 26 (1991) 6741–6752.
[44] K. Bangyikhan, Effects of oxide film, Fe-rich phase, porosity and their interactions on tensile properties of cast Al–Si–Mg alloys, University of Birmingham, Birmingham, 2005.
[45] T. Hauck, C. Bohm, W.H. Muller, Proceedings of the 6th. International Conference on Thermal, Mechanical and Multiphysics Simulation and Experiments in Micro-Electronics and Micro-Systems, EuroSimE, IEEE, 2005, pp. 242–247.
[46] M. Tiryakioğlu, J. Campbell, Metall. Mater. Trans. A 41 (2010) 3121–3129.
[47] M. Tiryakioglu, D. Hudak, G. Okten, Mater. Sci. Eng. A 527 (2009) 397–399.